Journal of
Mechanics of
Materials and Structures

PREDICTION OF SPRINGBACK AND RESIDUAL STRESS OF A BEAM/PLATE SUBJECTED TO THREE-POINT BENDING

Quang Khoa Dang, Pei-Lun Chang, Shih-Kang Kuo and Dung-An Wang

Volume 13, No. 4 July 2018

msp

JOURNAL OF MECHANICS OF MATERIALS AND STRUCTURES
Vol. 13, No. 4, 2018
dx.doi.org/10.2140/jomms.2018.13.421

PREDICTION OF SPRINGBACK AND RESIDUAL STRESS OF A BEAM/PLATE SUBJECTED TO THREE-POINT BENDING

QUANG KHOA DANG, PEI-LUN CHANG, SHIH-KANG KUO AND DUNG-AN WANG

A model for prediction of springback and residual stress distribution of a beam/plate subjected to three-point bending and reverse bending is developed based on a mechanical-geometrical approach. A converged solution that satisfies both the Euler–Bernoulli beam theory and the geometrical constraints is obtained by a recursive scheme. The model can be applied to bending/unbending analyses of plates when the beam bending approaches a plane strain condition. Springback and residual stress distribution of a plate is predicted quite accurately by the model as verified by finite element analyses and experiments. Accuracy of springback and residual stress prediction of the model is examined with consideration of various geometry parameters of the beam and the fulcrum/support cylinders. The goal of this investigation is to develop an accurate and efficient model to predict the profile and residual stress of plates curved by bending in the postyield range. The developed model can serve as a unit cell of a more sophisticated model for leveling analyses of metal plates as multiple rollers are involved.

1. Introduction

Accurate estimation of springback and residual stress distribution of metal plates under leveling process is necessary for appropriate and efficient adjustment of the roller settings of the leveling machines. Development of an analytical model of the critical to the production process. The adjustment of the roller settings of the levelers is complicated and an efficient analytical model can assist the operators in obtaining high quality of the products. Levelers consist of rollers to deform sheet metal by alternative bending. The leveling process with multiple rollers can be viewed as a cyclic three-point bending process. An accurate three-point bending model with an efficient numerical algorithm is essential in implementing an analytical model of levelers to determine its relevant key characteristics. Three-point bending test was also designed to achieve a weight efficient structure of sandwiched beams [Li et al. 2011].

When modeling three-point bending, a beam subjected to displacements of a punch cylinder contacts the punch cylinder and two fulcrum cylinders tangentially and does not penetrate cylinder surface. Conway [1947] and Theocaris et al. [1977] investigated deflections of beams under three-point bending by elliptical integrals method. Ohtsuki [1986] analyzed large deflection bending stress of an elastic beam under three-point bending based on a Legendre–Jacobi form's elliptic integrals. Arnautov [2005] also adopted elliptical integrals to provide a bending stress solution to the problem. Batista [2015] gave an equilibrium configuration of an elastic beam subjected to three-point bending in terms of Jacobi elliptical functions. Deflection behaviors of beams under three-point bending have also been investigated by classical beam theory [Mujika 2006; Mohyeddin and Fereidoon 2014]. These solutions of the three-point bending problems were obtained by assuming elastic behavior of the beam material. Considering material

Keywords: springback, residual stress, three-point bending, beam, plate.

hardening in the analyses, Hill [1950] and Gao [1994] derived solutions of pure bending of beams by assuming elastic, linear plastic material. Pure bending of a plate made of a power-law-hardening material was studied by Triantaflyllidis [1980] and Zhu [2007]. Kang and Li [2009] investigated bending stress of a cantilever beam with power-law nonlinearity.

Prediction of final shape of beams/plates is a complex task in metal forming industries. Residual stress distribution of beams/plates after springback has a strong influence on their final shape. Analytical solutions for springback of beams and plates under pure bending were developed by Johnson and Yu [1981]. Lin and Hua [2000] developed an analytical method to compute large deflection and springback of a thin plate with strain hardening under four-roll bending process. Gergess and Sen [2016] derived closed form solutions of load to deformation relation and profiles of steel members under point bending. For more complex bending problems, however, numerical techniques are adopted. Sitar et al. [2015] presented a numerical procedure to compute springback of beams with asymmetric cross-sections. Zhang et al. [2007] developed a model to predict springback of sheet metals after U-bending. They applied kinematic, isotropic, and combined hardening laws in their model to account for stretching, bending, and unbending of sheet metals during the U-bending process. Chiew et al. [2016] employed a numerical modeling procedure to obtain residual stress distribution of steel members produced by three-roller bending. They proposed a residual stress model to predict residual stress distribution of the curved member. Kuwabara et al. [1996] presented an analytical model to predict the amount of springback of a sheet metal subjected to bending-unbending under tension. Given the curvatures of the sheet metal before the deformation process, they calculated the residual stress distribution and residual curvature of the sheet metal at the point of interest. Takahashi et al. [1996] performed a die bending test to verify the calculated residual curvature by Kuwabara et al. [1996]. Kuwabara et al. [1999] established a numerical analysis method for analyzing bending/unbending process of sheet metal at the point of interest. Their model incorporates a three-dimensional constitutive model and the Ziegler's kinematic hardening model.

In this investigation, a one-dimensional model of three-point bending tests capable of calculating path/curvature of beams/plates, induced stress/strain histories, and hence final residual stress distribution is developed. The stress/curvature distribution along the span of the beams/plates over the supports can be calculated by the model. This model can be extended to simulate roller leveling process, which can be approximated by a sequence of three-point bends between rollers. A phenomenological combined hardening parameter is adopted to take isotropic and kinematic hardening into account during reverse bending. In the model, support contact is incorporated into the pure bending problem of beams under three-point bending in order to obtain springback and residual stress solutions. A recursive scheme considering Euler–Bernoulli beam theory and geometrical constraints is adopted to obtain converged solutions of beams under three-point bending and reverse bending. The model with consideration of the

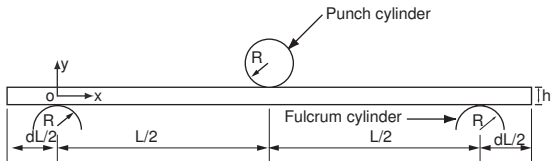

Figure 1. A schematic of a three-point bending test and a Cartesian coordinate system.

material strain hardening is based on proportional straining conditions. Two-dimensional, plane strain finite element analysis of beams subjected to three-point bending and reverse bending is carried out to verify the model. The analysis is performed for various displacement loadings as well as different values of radius of fulcrum cylinders. Experiments of three-point bending are performed to test the applicability of developed analytical model. Finally, discussions and conclusions are given.

2. Model

Besides the assumptions of Euler–Bernoulli beam theory, friction forces at the roller supports, longitudinal forces along the beam, gravity, and span shortening caused by deflection are neglected in the numerical model. Figure 1 schematically shows a three-point bending test of a beam. The beam has a length of $L + dL$, a thickness of h and a width of w. The overhang length of the beam is $dL/2$. The radius of the punch cylinder and fulcrum cylinders is R. A Cartesian coordinate system is also shown in the figure, where x represents the longitudinal direction, y represents the thickness direction, and z is the width direction of the beam. The origin of the y coordinate is at the middle of the beam as shown in the figure. Longitudinal strain ε_x can be written as

$$\varepsilon_x = -\kappa y, \tag{1}$$

where ε_x is the longitudinal strain, and κ represents the curvature. Large deflection of beams under three-point bending may induce significant plastic deformation in the beam material. It is critical to study the large plastic deformation of beams under three-point bending. When the beam is considered as an elastic-linear plastic material, the effective stress $\bar{\sigma}$ is given as

$$\bar{\sigma} = \sigma_0 + E_p(\bar{\varepsilon} - \sigma_0/E), \tag{2}$$

where σ_0 is the yield stress and $\bar{\varepsilon}$ is the effective total strain. E and E_p are the Young's modulus and plastic modulus, respectively. Assuming the von Mises criterion and plane-strain condition apply, the stress in the width direction σ_z is

$$\sigma_z = \tfrac{1}{2}(\sigma_x + \sigma_y), \tag{3}$$

where σ_x and σ_y are the stresses in the longitudinal direction and thickness direction, respectively. Under pure bending, the stress in the thickness direction σ_y is negligible, and the effective stress $\bar{\sigma}$ is

$$\bar{\sigma} = \tfrac{\sqrt{3}}{2}|\sigma_x|. \tag{4}$$

Assuming volume conservation and plane-strain condition apply, the effective total strain can be expressed as

$$\bar{\varepsilon} = \tfrac{2}{\sqrt{3}}|\varepsilon_x|. \tag{5}$$

As described by Hill [1950] and Zhu [2007], the volume conservation is needed here to solve exactly the pure bending problem of beams or plates in the elastic and plastic region. Relatively large plastic deformation is considered in this investigation. This assumption contributes to a very small fraction of error to the results. Because of symmetry, the bending moment M is given as

$$M = -2w\int_0^{h/2} \sigma_x y\, dy. \tag{6}$$

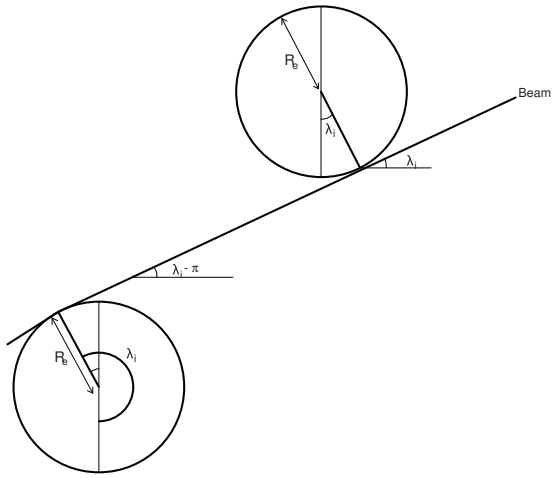

Figure 2. A schematic of cylinders below and above the beam.

The sign convention for the moment M and the curvature κ is related to the orientation of the coordinate axes.

In order to estimate the contact points at which the beam contacts with the cylinders, it is assumed that the beam contacts each cylinder tangentially as shown in Figure 2. As seen in the figure, R_e is the expanded radius of the roller and is given as

$$R_e = R + \tfrac{1}{2}h. \tag{7}$$

The gradient of the longitudinal axis of the beam is equal to the tangent of the contact angle λ_i as [Müller et al. 2013]

$$\left.\frac{dy}{dx}\right|_{x_i} = \tan\lambda_i, \tag{8}$$

where $y(x)$ is the longitudinal axis of the beam, (x_i, y_i) is the i-th contact point, and λ_i is the i-th contact angle. The contact point (x_i, y_i) can be expressed as

$$x_i = x_c + R_e \sin\lambda_i, \quad y_i = y_c - R_e \cos\lambda_i, \tag{9}$$

where (x_c, y_c) is the coordinates of the center of the punch/fulcrum cylinder.

The curvature, bending moment, deflected curve of the beam, and the contact points may be determined through a recursive scheme. First, the location of the three contact points and the beam curvature κ_i at the i-th contact point are assumed. The bending moment M_i at the i-th contact point is computed based on (1)–(6). Neglecting weight of the beam, the bending moment at the two fulcrum cylinders can be taken as zero and it has an extreme value at the punch cylinder. The curvature of the deflected beam is estimated based on the linear distribution of the bending moment between the fulcrum cylinder and the punch cylinder. Once the curvature distribution $\kappa(x)$ is known, the beam profile is given by

$$y(x) = \iint \kappa(x)\,dx + C_1 x + C_2, \tag{10}$$

parameters	value
Poisson's ratio	0.33
Young's modulus (GPa)	70.3
tensile strength (MPa)	175.1
plastic modulus (MPa)	1579

Table 1. Material properties for AA5052.

where the constants C_1 and C_2 can be determined by the contact points at the fulcrum cylinders. The recursive scheme is shown in Figure 3. A converged solution of the beam profile, moment distribution, curvature distribution, and contact points that satisfies both the Euler–Bernoulli beam theory and the geometrical constraints can be obtained by the recursive scheme. The recursive scheme outlined in Figure 3 is based on a procedure presented by Higo et al. [2016]. Pure bending moment/curvature equation has been used to simulate deflections of beams with elastoplastic behavior [Natarajan and Peddieson 2011]. Pandit and Srinivasan [2016] described a method to analyze large deflections of a curved beam subjected to a tip-concentrated follower load. Based on a linearly hardening model, they obtained a moment-curvature constitutive law for their bending problem.

As the punch cylinder is lifted and loses contact with the beam, the beam springs back elastically and the internal stress distribution results in a zero bending moment. Assuming no reverse yielding during unloading, the curvature after unbending κ' can be expressed as [Hosford and Caddell 1993]

$$\kappa' = \kappa - M/(EI), \tag{11}$$

where κ and M are the curvature and moment, respectively, before springback, and I is the second moment of inertia of the beam cross section.

Finite element analyses are carried out to verify the simple model for springback estimation of the beam. The commercial software ABAQUS is used in this investigation. Due to the symmetry, only the right half of the specimen is modeled. The finite element model is shown in Figure 4 (top). The punch cylinder and the right fulcrum cylinder are also schematically shown in the figure. Two-dimensional plane strain 4-noded CPE4R elements are used in the model. The number of elements is 8436 in the finite element model. Figure 4 (bottom) is a close up view of the mesh near the punch cylinder. The finite element mesh is made denser in the region under the punch and over the fulcrum. In ABAQUS, the "rigid surface" option is used to describe the punch cylinder and the fulcrum cylinders, and the "contact pair" option is used to describe the contact between the punch and the fulcrums with the beam. The displacement of the rigid punch is controlled in the analyses. The material properties for AA5052 aluminum alloy used in this investigation are listed in Table 1. Figure 5 shows a stress-strain curve for the AA5052 from tensile tests. The plastic modulus of the elastic linear plastic material behavior of the AA5052 is taken as the slope of the fitted line shown in the figure. The strain is up to 0.025 during the tensile tests. As seen in Figure 5, the stress at this strain value only goes to about 200 MPa. The stress is computed by a linear extrapolation scheme for the strain higher than 0.025. The model can be applied to various metals with specified strain hardening behaviors.

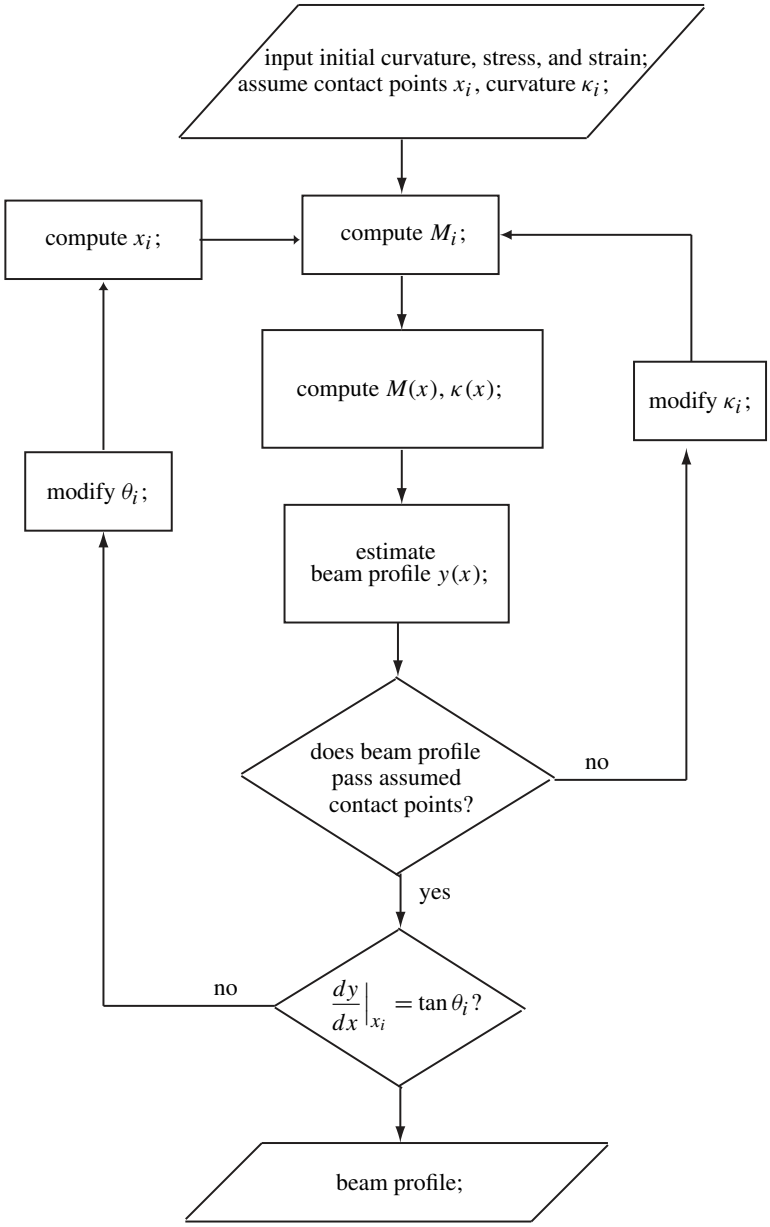

Figure 3. A recursive scheme.

3. Numerical results

The beam considered in this investigation has a length of 400 mm, a width of 100 mm, and a thickness of 6 mm. The overhang length of the beam $dL/2$ is 60 mm. The radius of the punch cylinder and fulcrum cylinders is 1 mm. Finite element computational results are used to evaluate the applicability of the developed model. Table 1 lists the material properties for the beam material, AA5052, with elastic linear

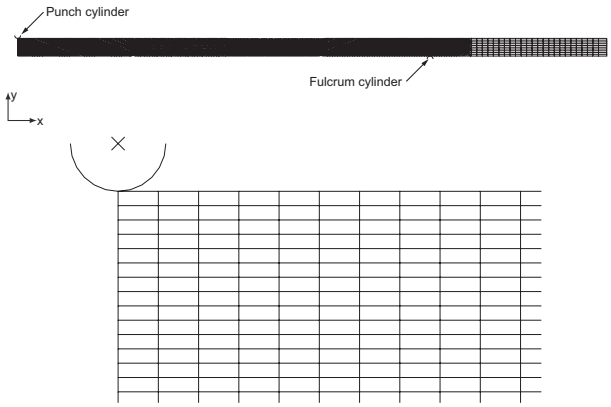

Figure 4. Top: a finite element model for the right half of a specimen. Bottom: a close up view of the mesh near the punch cylinder.

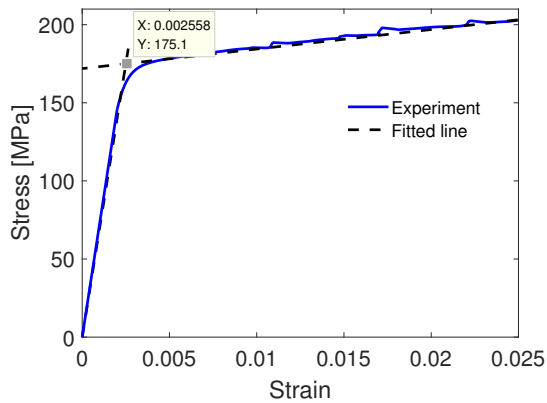

Figure 5. Tensile stress-strain curve for the AA5052 aluminum alloy.

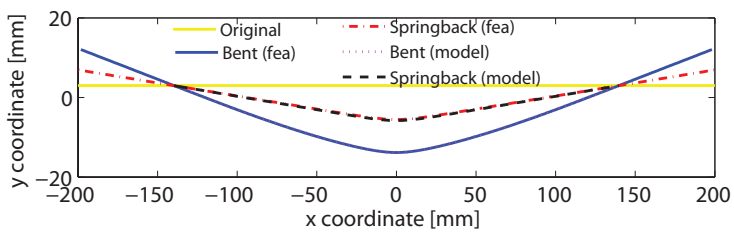

Figure 6. Beam profiles after bending and springback based on computational results of the model and FEA.

plastic material behavior. Computational grids of the analytical model are taken as 40 and 100 in the thickness direction and the longitudinal direction of the beam, respectively. The downward displacement of the punch cylinder is 16.81 mm.

Figure 6 shows the computational results based on the model (model) and the finite element analyses (fea). Seven contact point iterations and five contact angle iterations are required to reach a converged

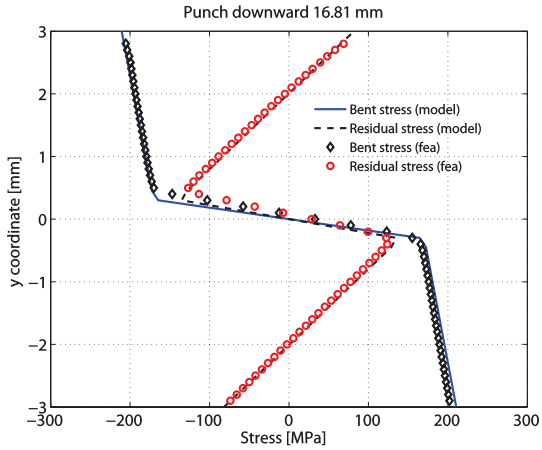

Figure 7. Stress distributions across beam thickness based on the model and the finite element analyses.

solution. The code based on the model takes 2.82 seconds to run on an AMD Phenom II X2 550 3.10 GHz processor. As seen in the figure, the beam profile after bending based on computational results of the model agrees with that based on the finite element analyses. The beam profile based on the model is estimated by the double integral of the curvature as in (6). The agreement between the model and the finite element analyses demonstrates the feasibility of the recursive scheme for calculation of the moment distribution and curvature distribution of the beam under three-point bending. The beam profile after springback is also shown in Figure 6. The displacements of the center of the beam due to springback based on the model and the finite element analyses are 8.02 mm and 8.28 mm, respectively. The percentage error in the springback estimation between the model and the finite element analyses is nearly 3%. The beam profile after springback predicted by the model is very close to that based on the finite element analyses.

After unloading, elastic springback occurs, and considerable residual stress results. Figure 7 shows the longitudinal stress distributions across beam thickness at the center of the beam based on the model and the finite element analyses. After bending and unloading, the stress σ_x based on the model agrees well with the finite element analyses. The stress distribution in the elastic region is a straight line with a slope of $1/(\kappa E)$. As seen in the figure, the slopes of the lines based on the model are slightly less than those based on the finite element analyses. This may be because the curvature κ in the model is approximated by $\kappa \approx d^2y/dx^2$, and the curvature of a plane curve $y = y(x)$ is

$$\kappa = \frac{d^2y/dx^2}{(1 + (dy/dx)^2)^{3/2}}. \tag{12}$$

The applicability of the developed model for springback and residual stress distribution for beams under three-point bending is verified by the finite element analyses. The cases of plates under three-point bending can be approached by the plane strain condition considered in the derivation of the model.

Figure 8. A photo of a three-point bending setup for beam specimens.

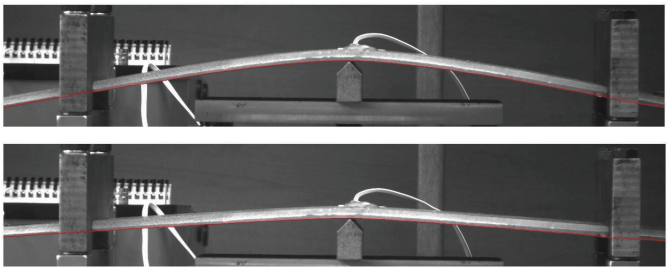

Figure 9. Photos of a beam specimen: after bending (top) and springback (bottom).

4. Experiments and results

Specimens used in experiments were fabricated with AA5052 aluminum alloy. The material properties of AA5052 aluminum alloy are listed in Table 1. The specimens were loaded in a three-point bending setup. A photo of the three-point bending setup is shown in Figure 8. It is seen that the punch cylinder is placed under the specimen and can be moved upward and downward by turning a knob under the punch cylinder. The beam specimens used in this investigation have a width of 100 mm and a length of 400 mm. The thickness of the beam specimens is 6 mm. The radius of the punch cylinder and fulcrum cylinder is 1 mm. The distance L between the two fulcrums is 280 mm. The length of the two overhangs is 60 mm. The loading rate of the punch was 5 mm per minute. A video camera was used to record the deformation of the beam specimens on one side of the beam specimens. A strain gauge was attached to the top surface of the beam specimen. Loading was applied by the punch cylinder until the desired displacement of the punch was reached. The displacement of the punch was controlled by reading the output of the strain gauge. In this investigation, the displacement of the punch was set as 16.81 mm.

Figure 9 (top and bottom) shows photos of a beam specimen after bending and springback, respectively. Three tests were performed and the photos of the specimen profiles were taken by the camera. Figure 10 shows the beam profiles after bending and springback based on computational results of the model and the experiments. The experimental results show some discrepancies due to the alignment error of the experimental setup and sliding between the beam specimens and the punch/fulcrum cylinders. One of

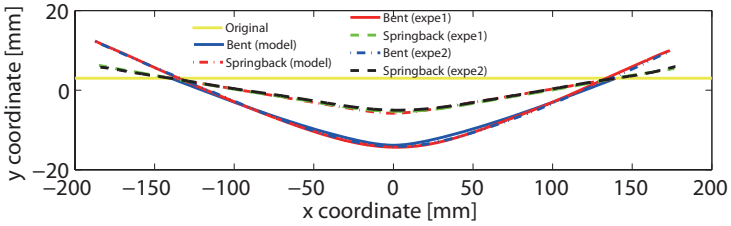

Figure 10. Beam profiles after bending and springback based on computational results of the model and experiments.

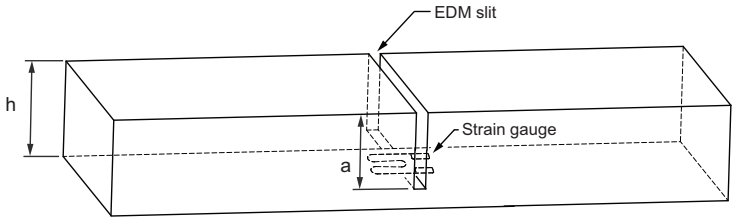

Figure 11. A schematic of the slitting method.

the three experimental results was discarded since it deviates from the other two experimental results in a greater amount. The average amount of springback at the center of the beam based on the two experimental results is 8.66 mm. Compared to the springback amount based on the model, 8.02 mm, the error in springback estimation of the model is 7%. This discrepancy can be accepted considering the alignment/measurement errors and sliding between specimens and punch/fulcrum cylinders during experiments.

The residual stress of the bent beam was measured by a slitting method [Schajer and Prime 2006]. Figure 11 is a schematic of the slitting method. In the figure, a represents the depth of the slit. A strain gauge is attached to a surface opposite to the slit. The method is based on the principle that residual stress causes a body to deform when it is cut. The deformation is measured by strain gauges while cutting progressively through the body. The strain record allows calculation of the residual stress distribution. In this investigation, a slit was cut by electrical discharge machining (EDM) through the thickness direction at the center of the specimen to a final depth of 5.33 mm (0.89% of specimen thickness). Strain at each depth was measured by strain gauges. Residual stress results were obtained by the pulse stress function and regularization as described in Schajer and Prime [2006]. Figure 12 shows the residual stress distributions in the thickness direction at the center of the specimen based on the model and the experiment. The stress results based on the model have good agreement with the stresses measured by the slitting method.

In order to explore the feasibility of the developed model for estimation of profile and residual stress of specimens subjected to three-point bending, the effects of punch displacement on the amount of springback after unloading are examined. The values of the material constants are listed in Table 1. Figure 13 shows the error in springback as a function of the normalized punch displacement for the aluminum material. The normalized punch displacement ranges from 1 to 5. The punch displacement is normalized by the specimen thickness. The percentage error in springback is calculated by the difference

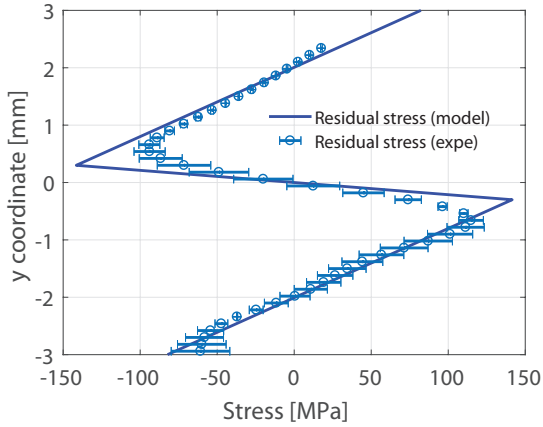

Figure 12. Residual distributions across beam thickness based on the model and the experiments.

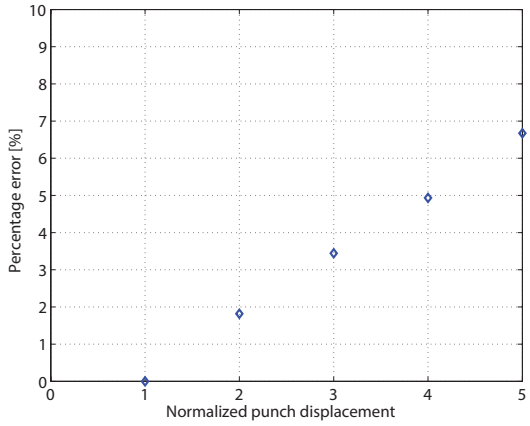

Figure 13. Percentage error in springback as a function of the normalized punch displacement.

in the springback at the center of the specimen between the model and the finite element analyses divided by that of the finite element analyses. As shown in the figure, the error increases almost linearly as the normalized punch displacement increases. At the normalized punch displacement of 5, the springback amount predicted by the model has a percentage error of 6.7%.

Figure 14 shows the stress distributions at various punch displacements ranging from 6 mm to 30 mm, corresponding to the normalized punch displacements ranging from 1 to 5. Due to the pressure of the punch cylinder on the top surface of the specimen in the finite element analyses, a stress concentration region is located near the contact point at the top surface of the specimen. Therefore, the longitudinal stresses near the top surface of the specimen based on the finite element analyses are erroneous. The stress after bending and the residual stress after springback computed by the model agree with those based on the finite element analyses. The yielding fraction of the beam thickness is 31 % when the punch displacement is 6 mm. The yielding fraction reaches 90 % when the punch displacement is 30 mm. The model provides a relatively accurate estimation of the residual stress distributions under three-point bending.

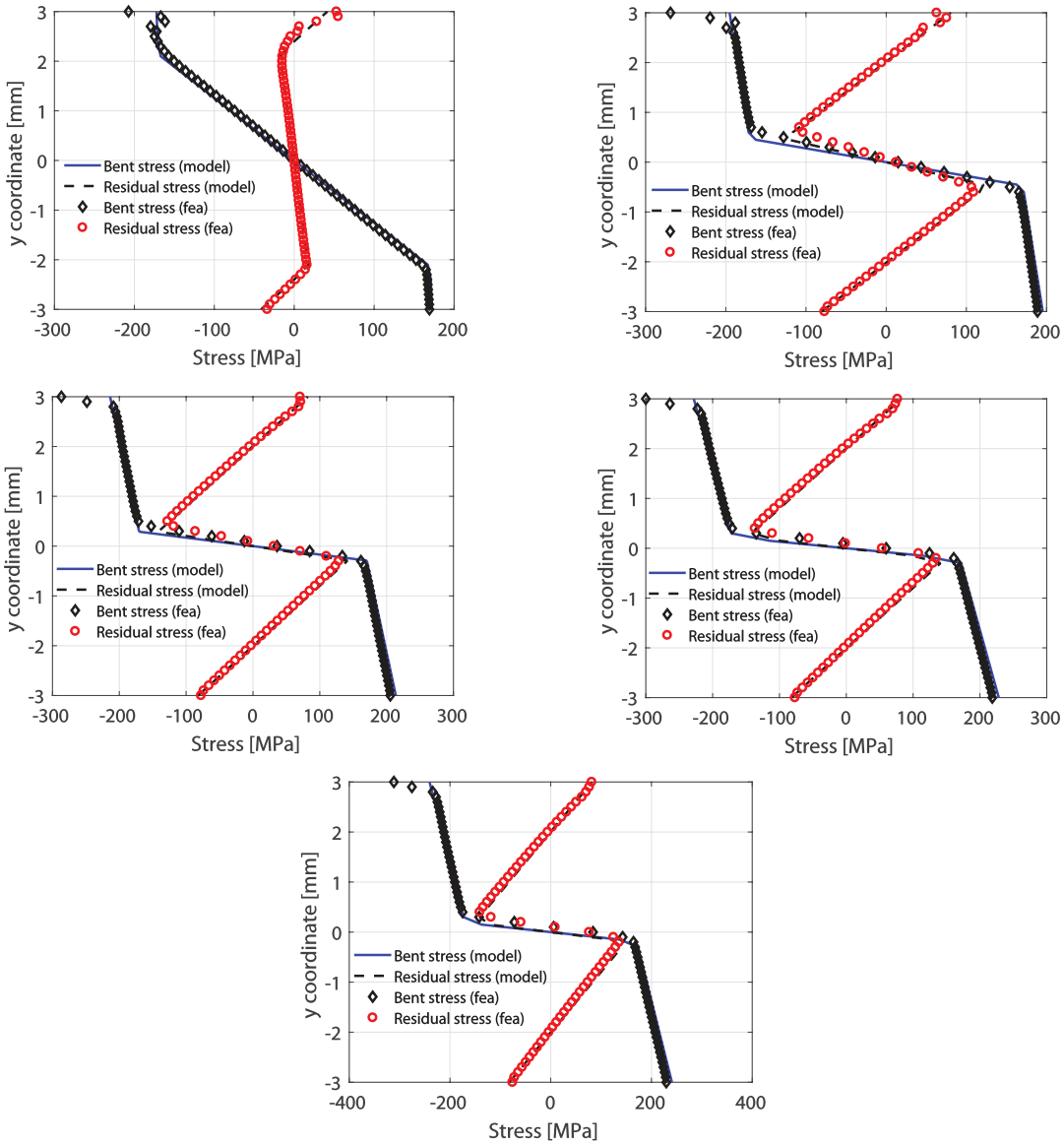

Figure 14. Stress distributions across beam thickness based on the model and the finite element analyses at the punch displacement of 6 mm (top left), 12 mm (top right), 18 mm (center left), 24 mm (center right), and 30 mm (bottom).

The position of contact point of the specimen with the fulcrum cylinders varies as the specimen rolls over the fulcrum cylinders during three-point bending tests. When the contact points changes significantly, the position of the contact point has a major effect on the specimen profiles after springback. An analytical model should be able to model the position of the contact point accurately and efficiently. Figure 15 shows the percentage error of the springback prediction of the model for different normalized radii of the fulcrum radius. The downward displacement of the punch cylinder is 16.81 mm. The fulcrum

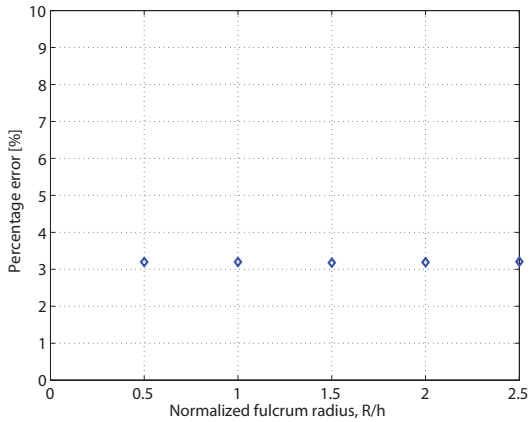

Figure 15. Percentage error in springback as a function of the normalized fulcrum radius.

radius R is normalized by the specimen thickness h. The percentage error is the difference between the model prediction and computed value of the finite element analyses divided by the value of the finite element analyses and is given as a percent. For the considered R/h values of 0.5, 1, 1.5, 2, 2.5, the percentage errors are nearly 3%. When the $R/h = 2.5$ and the downward displacement of the punch is 16.81 mm, the rotation of the beam over the fulcrum cylinders is 8.75°. For the R/h ratios considered, the model provides acceptable prediction of the springback of the beam under three-point bending compared to the results based on the finite element analyses.

Figure 16 and Figure 17 show the specimen's profiles and residual stress distributions, respectively, after bending and springback based on the model and the finite element analyses for various values of the normalized radius of the fulcrum cylinder. The profiles after springback and the residual stress distributions predicted by the model are in good agreement with those based on the finite element analyses. Note that the stresses near the top surface of the specimen are erroneous due to the stress concentration caused by the pressure from the punch cylinder in the finite element analyses, where the stress gets much larger than that predicted by the model.

Reverse bending has practical importance in sheet forming processes. A reverse bending process is investigated in order to verify the possibility to utilize the present model to leveling processes. Figure 18 (top) shows a setup of a three-point bending test considered in the model. The setup for reverse bending is schematically shown in Figure 18 (bottom). The curvature and deflected curve of the beam after bending and reverse bending are determined by the recursive scheme as shown in Figure 3. The curvature and stress distributions of the beam after the bending process are taken as the initial curvature and stress during the reverse bending process. Assuming isotropic hardening and using (1)–(6) and (11), the stress distributions after reverse bending and springback can be computed.

Due to the constraint of the available experimental apparatus, a reverse bending and springback experiment cannot be performed. Finite element analysis is sought to verify the deflected curve and stress distributions obtained by the model. Figure 19 (top) shows a schematic of a finite element model where two punches are in contact with the center of the beam. Two pairs of vertically aligned fulcrums are located near the left end and right end of the beam, a left pair and a right pair, respectively. Figure 19 (second row) is a schematic of the finite element model during bending. During reverse bending of

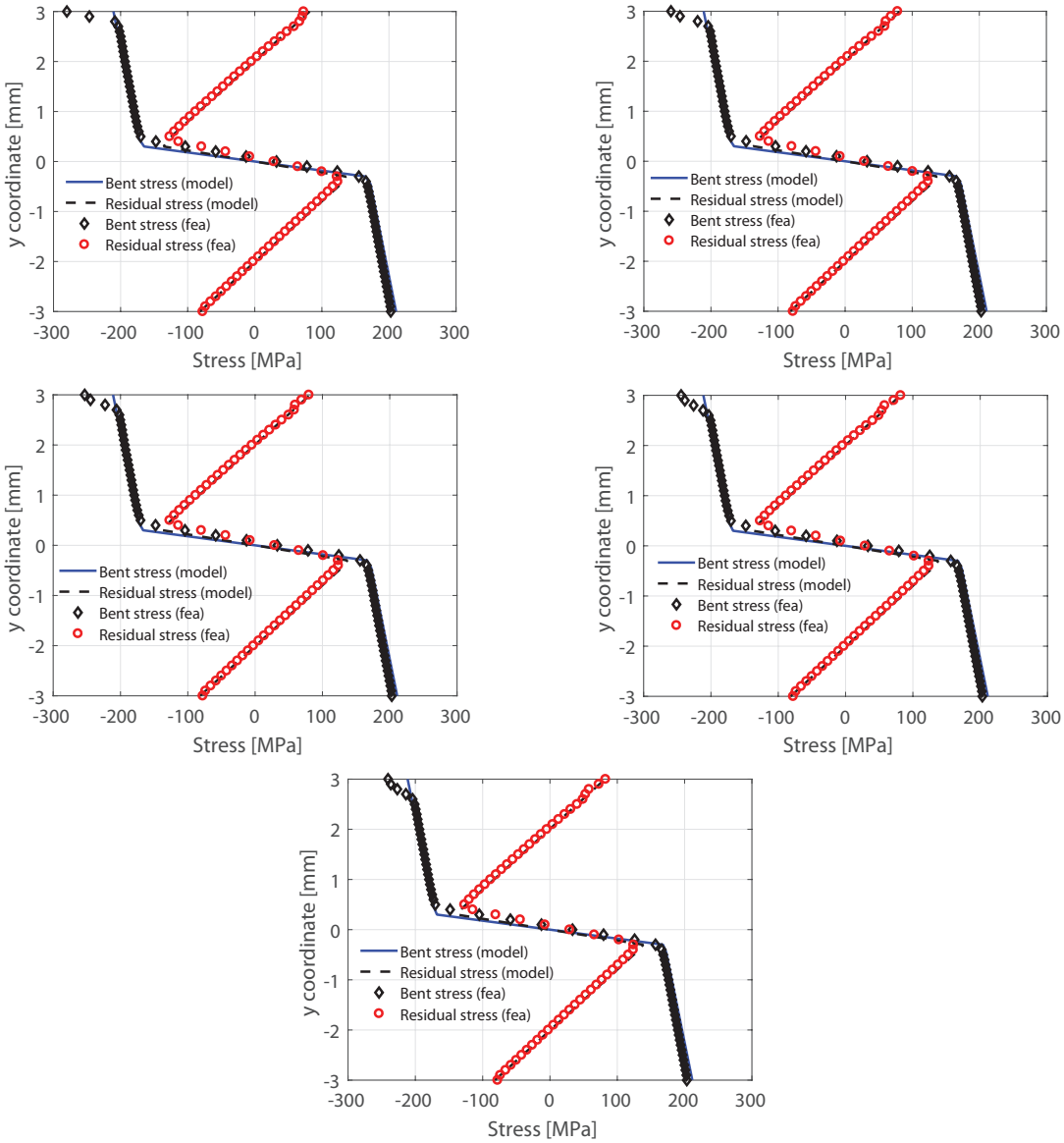

Figure 16. Beam profiles after bending and springback based on computational results of the model and finite element analyses at various values of the normalized radius of the fulcrum cylinder of 0.5 (top left), 1 (top right), 1.5 (center left), 2 (center right), and 2.5 (bottom).

the finite element analysis, the lower fulcrums of the left pair and the right pair and the upper punch are removed; see Figure 19 (third row). The lower punch is removed for the springback analysis; see Figure 19 (bottom).

In the analysis, the punch is moved downward 16.81 mm then moved upward 16.81 mm for bending and reverse bending, respectively. The radius of the punch and the fulcrum is taken as 1 mm. The beam

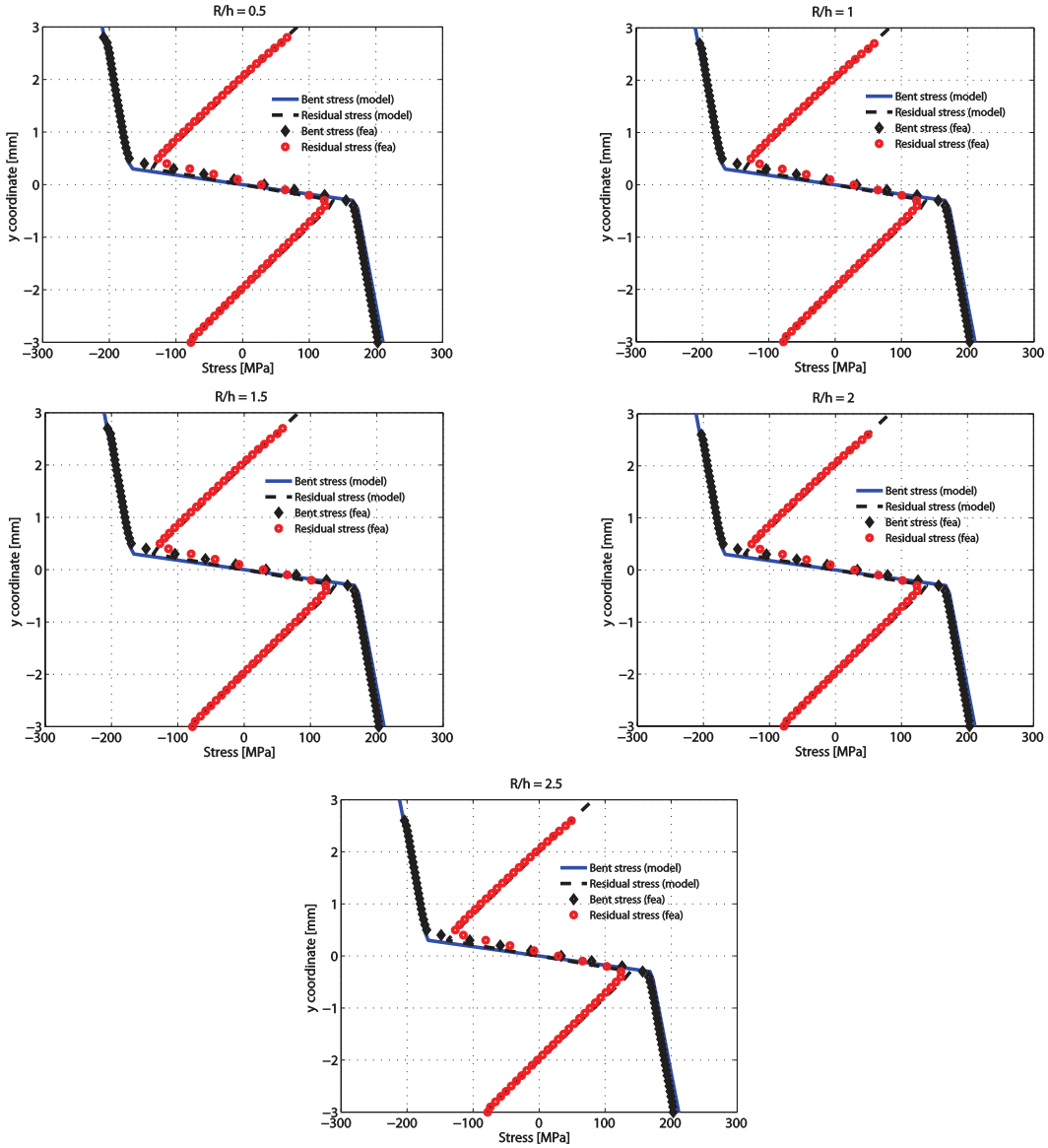

Figure 17. Stress distributions across beam thickness based on the model and the finite element analyses at the normalized fulcrum radius of 0.5 (top left), 1 (top right), 1.5 (center left), 2 (center right), and 2.5 (bottom).

has a length of 400 mm, a width of 100 mm and a thickness of 6 mm. Figure 20 (top) shows the meshes of the finite element model of the right half of the beam in its initial configuration. The meshes after bending, reverse bending, and springback are shown in second row, third row, and bottom of Figure 20, respectively.

Figure 21 shows the specimen's profiles after reverse bending and springback based on the model and the finite element analyses. The profiles after reverse bending and springback predicted by the model

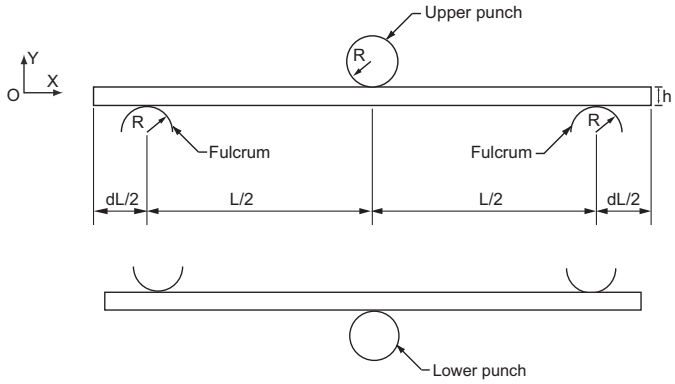

Figure 18. Schematics of: a three-point bending setup (top) and a three-point reverse bending setup (bottom).

are in good agreement with those based on the finite element analyses. Figure 22 shows the stress distributions after reverse bending and springback based on the model and the finite element analyses. The residual stress distributions predicted by the model agree with those based on the finite element analyses.

For materials that exhibit a combined isotropic and kinematic hardening behaviors, the yield stress in reverse loading is usually lower than that in the case of continuous loading. During the three-point

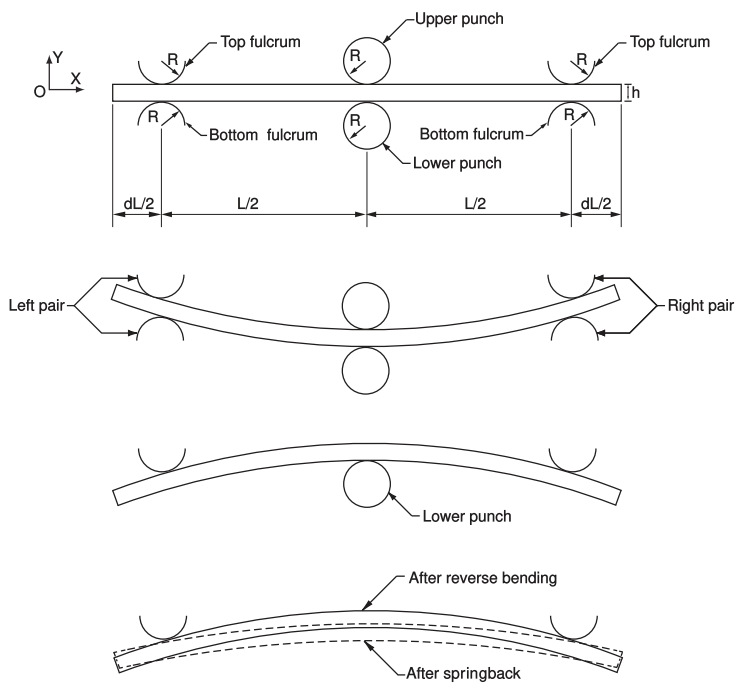

Figure 19. Schematics of a finite element model where two punches are in contact with the center of the beam.

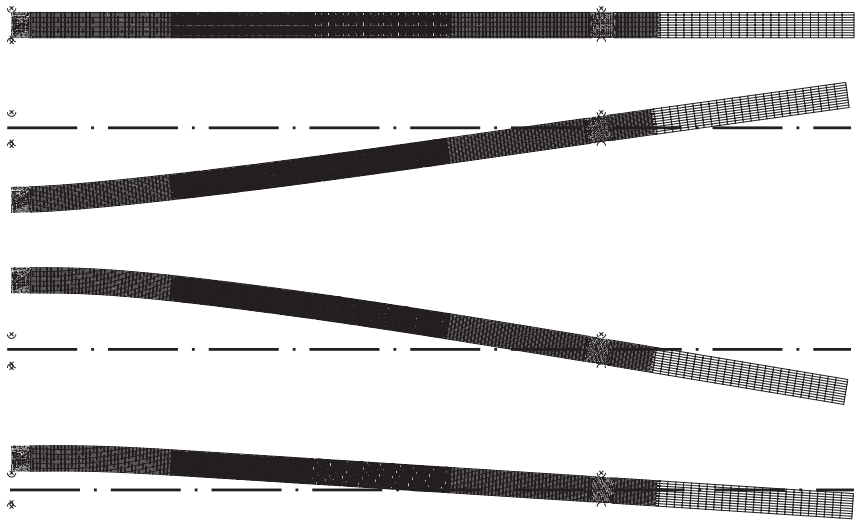

Figure 20. Meshes of the finite element model of the right half of the beam: in its initial configuration (top), after bending (second row), after reverse bending (third row), and after springback (bottom).

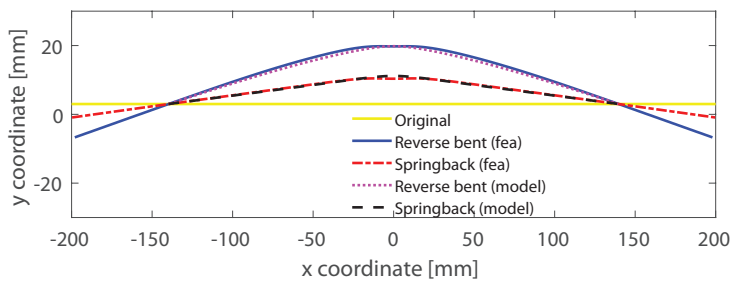

Figure 21. Beam profiles after reverse bending and springback based on the model and the finite element analyses.

reverse bending, the isotropic hardening model is no longer an adequate approximation. Therefore, under reverse bending, consideration of a combined hardening model is required for prediction of a realistic stress distribution and springback [Geng et al. 2002]. In order to extend the applicability of the developed model in roller leveling process, a phenomenological combined hardening parameter is adopted to take isotropic and kinematic hardening into account during reverse bending. Under reverse bending condition, change in effective stress $\Delta\bar{\sigma}$ can be given as [Zhang et al. 2007]

$$|\Delta\bar{\sigma}| = \begin{cases} E|\Delta\bar{\varepsilon}| & |\Delta\bar{\varepsilon}| < |\Delta\bar{\sigma}|_{\text{lim}}/E, \\ \sigma_0 + E_p(|\Delta\bar{\varepsilon}| - |\Delta\bar{\sigma}|_{\text{lim}}/E) & |\Delta\bar{\varepsilon}| \geq |\Delta\bar{\sigma}|_{\text{lim}}/E, \end{cases} \tag{13}$$

where $|\Delta\bar{\varepsilon}|$ is the absolute value of the change in effective total strain from the initial loading point to the current loading point during reverse bending; $|\Delta\bar{\sigma}|_{\text{lim}}$ is the limiting value of effective stress change

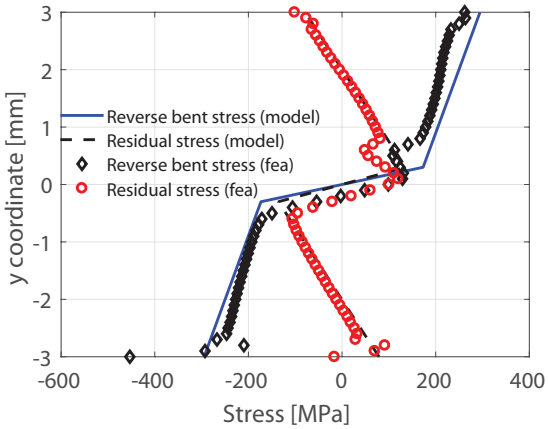

Figure 22. Stress distributions across beam thickness after reverse bending and springback based on the model and the finite element analyses.

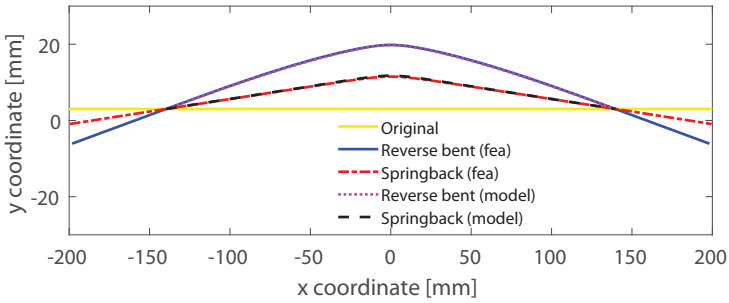

Figure 23. Beam profiles after reverse bending and springback based on the model and the finite element analyses for the case of kinematic hardening.

in the elastic regime after reverse bending and is written as

$$|\Delta\bar{\sigma}|_{\text{lim}} = (1+m)|\bar{\sigma}_r| + (1-m)(2\sigma_0 - |\bar{\sigma}_r|), \tag{14}$$

where $|\bar{\sigma}_r|$ is the absolute value of effective stress when the reverse bending occurs and m is a combined hardening coefficient. The value of m can be taken as 1 or 0 corresponding to isotropic hardening or kinematic hardening, respectively. For combined isotropic and kinematic hardening, the value of m is between 0 and 1.

Assuming kinematic hardening during reverse bending, the feasibility of the present model for materials with kinematic hardening is investigated. Using (1)–(6), (11), and (13)–(14) with $m = 0$, the stress distributions after reverse bending and springback can be computed. Figure 23 shows the specimen's profiles after reverse bending and springback based on the model and the finite element analyses for the case of kinematic hardening. Good agreement is obtained between model results and finite element analyses results. Figure 24 shows the stress distributions after reverse bending and springback based on the model and the finite element analyses for the case of kinematic hardening. The stress results obtained from the model show good agreement with those based on the finite element analyses.

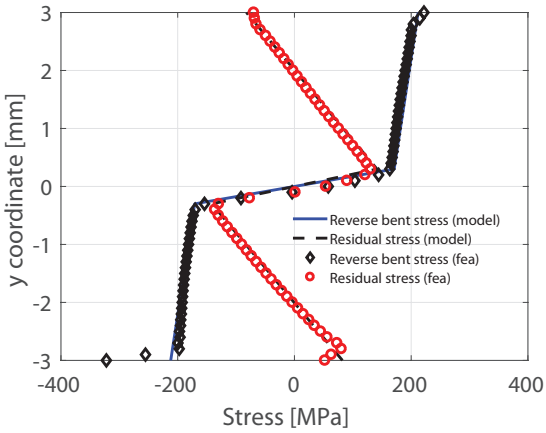

Figure 24. Stress distributions across beam thickness after reverse bending and springback based on the model and the finite element analyses for the case of kinematic hardening.

It is noted that the bending/unbending model presented by Kuwabara et al. [1996] can predict the residual curvature relatively accurately and their model was compared with results of finite element analyses in draw-bending processes by Hama et al. [2008]. Compared to the model presented in this investigation, Kuwabara's model is more sophisticated with the consideration of tension in bending processes and Ziegler's kinematic hardening law. The advantage of the present model is that it can calculate the residual stress and curvature distribution along the span of the beam over the supports. In the model, the deformed profile of the beam is obtained based on the curvature distribution and the combined isotropic and kinematic hardening during reverse bending is accounted for by a phenomenological combined hardening parameter. The model's prediction of the residual stress distribution and profile of the beam after bending and reverse bending is verified by experiments and finite element analyses.

5. Conclusions

A model for analyzing springback and residual stress distribution of beams under three-point bending is developed. Complex material hardening during bending and reverse bending can be modeled by a phenomenological combined hardening parameter in the model. The converged solutions of deflection and stress distribution of beams over the span of the supports under three-point bending and reverse bending with consideration of material plastic hardening behavior are computed very efficiently by the recursive scheme. Its feasibility to characterize the beam's profile and residual stress distribution after springback is verified by experiments and finite element analyses. The beam material is assumed to be elastic, linear plastic, and the plastic behavior of the beam is described by the von Mises yield criterion. Experimental results further confirm the accuracy of the model by comparing the experimental beam profiles and residual stress distribution after bending and springback with the results obtained by the model. Depending on the plastic behavior of the beam material, various hardening laws can be modeled and incorporated into the analytical model.

Since the multiroller leveling process of metal plates can be viewed as a series of bending/unbending of plates under three-point bending configurations, the developed model has the potential to be extended

to analyze the profile and residual stress of plates during the leveling process. Accuracy of the model for large deflection and relative large radius of fulcrum cylinders suggests that it is a reasonable building block for development of an analytical model of multiroller leveling of metal plates in steel mills.

Acknowledgements

This work was financially supported by China Steel Corporation (contract number: 05T1D-RE004). Partial support of this work given by a grant from Ministry of Science and Technology, Taiwan (grant number: MOST 105-2221-E-005-060) is greatly appreciated. The authors would like to express their appreciation to the National Center for High-performance Computing (NCHC), Taiwan, for their assistance.

References

[Arnautov 2005] A. K. Arnautov, "The method of three-point bending in testing thin high-strength reinforced plastics at large deflections", *Mech. Compos. Mater.* **41**:5 (2005), 467–476.

[Batista 2015] M. Batista, "Large deflections of a beam subject to three-point bending", *Int. J. Non-Linear Mech.* **69** (2015), 84–92.

[Chiew et al. 2016] S. P. Chiew, Y. F. Jin, and C. K. Lee, "Residual stress distribution of roller bending of steel rectangular structural hollow sections", *J. Constr. Steel Res.* **119** (2016), 85–97.

[Conway 1947] H. D. Conway, "XCIV. The large deflection of simply supported beams", *Lond. Edinb. Dubl. Phil. Mag. J. Sci.* **38**:287 (1947), 905–911.

[Gao 1994] X.-L. Gao, "Finite deformation elasto-plastic solution for the pure bending problem of a wide plate of elastic linear-hardening material", *Int. J. Solids Struct.* **31**:10 (1994), 1357–1376.

[Geng et al. 2002] L. Geng, Y. Shen, and R. H. Wagoner, "Anisotropic hardening equations derived from reverse-bend testing", *Int. J. Plast.* **18**:5-6 (2002), 743–767.

[Gergess and Sen 2016] A. Gergess and R. Sen, "Curving structural steel girders by two-point bending", *J. Constr. Steel Res.* **122** (2016), 511–519.

[Hama et al. 2008] T. Hama, T. Nagata, C. Teodosiu, A. Makinouchib, and H. Takuda, "Finite-element simulation of springback in sheet metal forming using local interpolation for tool surfaces", *Int. J. Mech. Sci.* **50**:2 (2008), 175–192.

[Higo et al. 2016] T. Higo, H. Matsumoto, and S. Ogawa, "Influence of delivery-side roll position of roller leveler to plate flatness", pp. 2129–2137 in 2016 *AISTech Conference Proceedings*, 2016.

[Hill 1950] R. Hill, *The mathematical theory of plasticity*, Oxford, Clarendon, 1950.

[Hosford and Caddell 1993] W. F. Hosford and R. M. Caddell, *Metal forming: mechanics and metallurgy*, Prentice Hall, 1993.

[Johnson and Yu 1981] W. Johnson and T. X. Yu, "On springback after the pure bending of beams and plates of elastic work-hardening materials, III", *Int. J. Mech. Sci.* **23**:11 (1981), 687–695.

[Kang and Li 2009] Y.-A. Kang and X.-F. Li, "Bending of functionally graded cantilever beam with power-law non-linearity subjected to an end force", *Int. J. Non-Linear Mech.* **44**:6 (2009), 696–703.

[Kuwabara et al. 1996] T. Kuwabara, S. Takahashi, and K. Ito, "Springback analysis of sheet metal subjected to bending-unbending under tension, I: Theory and results of numerical analysis", pp. 743–746 in *Advanced Technology of Plasticity* 1996*: Proceedings of the* 5*th International Conference on Technology of Plasticity* (Columbus, Ohio), edited by T. Altan, 1996.

[Kuwabara et al. 1999] T. Kuwabara, N. Seki, and S. Takahashi, "A rigorous numerical analysis of residual curvature of sheet metals subjected to bending-unbending under tension", pp. 1071–1076 in *Advanced Technology of Plasticity* 1999*: Proceedings of the* 6*th International Conference on Technology of Plasticity* (Nuremberg, Germany), edited by T. Gaiger, 1999.

[Li et al. 2011] M. Li, L. Wu, L. Ma, B. Wang, and Z. Guan, "Structural design of pyramidal truss core sandwich beams loaded in 3-point bending", *J. Mech. Mater. Struct.* **6** (2011), 1255–1266.

[Lin and Hua 2000] Y. H. Lin and M. Hua, "Influence of strain hardening on continuous plate roll-bending process", *Int. J. Non-Linear Mech.* **35**:5 (2000), 883–896.

[Mohyeddin and Fereidoon 2014] A. Mohyeddin and A. Fereidoon, "An analytical solution for the large deflection problem of Timoshenko beams under three-point bending", *Int. J. Mech. Sci.* **78** (2014), 135–139.

[Mujika 2006] F. Mujika, "On the difference between flexural moduli obtained by three-point and four-point bending tests", *Polym. Test.* **25**:2 (2006), 214–220.

[Müller et al. 2013] U. Müller, H. Krambeer, A. Wolff, A. Espina Viella, A. D. Richardson, J.-O. Perä, P. Luoto, and W. Weberm, "Optimisation of final plate flatness by set-up coordination for subsequent manufacturing process (final plate flatness)", Final report, EUR 25852 EN, European Commission, 2013, https://publications.europa.eu/en/publication-detail/-/publication/24f660f1-6532-4ce5-81c7-1b60389371a9.

[Natarajan and Peddieson 2011] A. Natarajan and J. Peddieson, "Simulation of beam plastic forming with variable bending moments", *Int. J. Non-Linear Mech.* **46**:1 (2011), 14–22.

[Ohtsuki 1986] A. Ohtsuki, "An analysis of large deflections in a symmetrical three-point bending of beam", *Bullet. JSME* **29**:253 (1986), 1988–1995.

[Pandit and Srinivasan 2016] D. Pandit and S. M. Srinivasan, "Numerical analysis of large elasto-plastic deflection of constant curvature beam under follower load", *Int. J. Non-Linear Mech.* **84** (2016), 46–55.

[Schajer and Prime 2006] G. S. Schajer and M. B. Prime, "Use of inverse solutions for residual stress measurements", *J. Eng. Mater. Technol.* (*ASME*) **128**:3 (2006), 375–382.

[Sitar et al. 2015] M. Sitar, F. Kosel, and M. Brojan, "Numerical and experimental analysis of elastic–plastic pure bending and springback of beams of asymmetric cross-sections", *Int. J. Mech. Sci.* **90** (2015), 77–88.

[Takahashi et al. 1996] S. Takahashi, T. Kuwabara, and K. Ito, "Springback analysis of sheet metal subjected to bending-unbending under tension, II: Experimental verification", pp. 747–750 in *Advanced Technology of Plasticity* 1996*: Proceedings of the* 5*th International Conference on Technology of Plasticity* (Columbus, Ohio), edited by T. Altan, 1996.

[Theocaris et al. 1977] P. S. Theocaris, S. A. Paipetis, and S. Paolinelis, "Three-point bending at large deflections", *J. Test. Eval.* **5**:6 (1977), 427–436.

[Triantaflyllidis 1980] N. Triantaflyllidis, "Bifurcation phenomena in pure bending", *J. Mech. Phys. Solids* **28**:3-4 (1980), 221–245.

[Zhang et al. 2007] D. Zhang, Z. Cui, X. Ruan, and Y. Li, "An analytical model for predicting springback and side wall curl of sheet after U-bending", *Comput. Mater. Sci.* **38**:4 (2007), 707–715.

[Zhu 2007] H. X. Zhu, "Large deformation pure bending of an elastic plastic power-law-hardening wide plate: analysis and application", *Int. J. Mech. Sci.* **49**:4 (2007), 500–514.

Received 21 May 2017. Revised 25 Sep 2018. Accepted 9 Oct 2018.

QUANG KHOA DANG: khoadq@hcmute.edu.vn
Graduate Institute of Precision Engineering, National Chung Hsing University, Taichung, Taiwan

PEI-LUN CHANG: iamalan1122@yahoo.com.tw
Graduate Institute of Precision Engineering, National Chung Hsing University, Taichung, Taiwan

SHIH-KANG KUO: 150359@mail.csc.com.tw
Iron and Steel Research and Development Department, China Steel Corporation, Kaohsiung, Taiwan

DUNG-AN WANG: daw@dragon.nchu.edu.tw
Graduate Institute of Precision Engineering, National Chung Hsing University, Taichung, Taiwan

JOURNAL OF MECHANICS OF MATERIALS AND STRUCTURES

msp.org/jomms

Founded by Charles R. Steele and Marie-Louise Steele

EDITORIAL BOARD

ADAIR R. AGUIAR	University of São Paulo at São Carlos, Brazil
KATIA BERTOLDI	Harvard University, USA
DAVIDE BIGONI	University of Trento, Italy
MAENGHYO CHO	Seoul National University, Korea
HUILING DUAN	Beijing University
YIBIN FU	Keele University, UK
IWONA JASIUK	University of Illinois at Urbana-Champaign, USA
DENNIS KOCHMANN	ETH Zurich
MITSUTOSHI KURODA	Yamagata University, Japan
CHEE W. LIM	City University of Hong Kong
ZISHUN LIU	Xi'an Jiaotong University, China
THOMAS J. PENCE	Michigan State University, USA
GIANNI ROYER-CARFAGNI	Università degli studi di Parma, Italy
DAVID STEIGMANN	University of California at Berkeley, USA
PAUL STEINMANN	Friedrich-Alexander-Universität Erlangen-Nürnberg, Germany
KENJIRO TERADA	Tohoku University, Japan

ADVISORY BOARD

J. P. CARTER	University of Sydney, Australia
D. H. HODGES	Georgia Institute of Technology, USA
J. HUTCHINSON	Harvard University, USA
D. PAMPLONA	Universidade Católica do Rio de Janeiro, Brazil
M. B. RUBIN	Technion, Haifa, Israel

PRODUCTION production@msp.org

SILVIO LEVY Scientific Editor

See msp.org/jomms for submission guidelines.

JoMMS (ISSN 1559-3959) at Mathematical Sciences Publishers, 798 Evans Hall #6840, c/o University of California, Berkeley, CA 94720-3840, is published in 10 issues a year. The subscription price for 2018 is US $615/year for the electronic version, and $775/year (+$60, if shipping outside the US) for print and electronic. Subscriptions, requests for back issues, and changes of address should be sent to MSP.

JoMMS peer-review and production is managed by EditFLOW® from Mathematical Sciences Publishers.

PUBLISHED BY

mathematical sciences publishers

nonprofit scientific publishing

http://msp.org/

© 2018 Mathematical Sciences Publishers

Journal of Mechanics of Materials and Structures

Volume 13, No. 4 July 2018

Prediction of springback and residual stress of a beam/plate subjected to three-point bending QUANG KHOA DANG, PEI-LUN CHANG, SHIH-KANG KUO and DUNG-AN WANG 421

Characterization of CNT properties using space-frame structure MUHAMMAD ARIF and JACOB MUTHU 443

Analytical approach to the problem of an auxetic layer under a spatially periodic load HENRYK KAMIŃSKI and PAWEŁ FRITZKOWSKI 463

Stability and nonplanar postbuckling behavior of current-carrying microwires in a longitudinal magnetic field YUANZHUO HONG, LIN WANG and HU-LIANG DAI 481

Three-dimensional Trefftz computational grains for the micromechanical modeling of heterogeneous media with coated spherical inclusions GUANNAN WANG, LEITING DONG, JUNBO WANG and SATYA N. ATLURI 505

Uniform stress resultants inside two nonelliptical inhomogeneities in isotropic laminated plates XU WANG, LIANG CHEN and PETER SCHIAVONE 531

An analytical solution for heat flux distribution of cylindrically orthotropic fiber reinforced composites with surface effect JUNHUA XIAO, YAOLING XU and FUCHENG ZHANG 543

Strain gradient fracture of a mode III crack in an elastic layer on a substrate JINE LI and BAOLIN WANG 555

Growth-induced instabilities of an elastic film on a viscoelastic substrate: analytical solution and computational approach via eigenvalue analysis IMAN VALIZADEH, PAUL STEINMANN and ALI JAVILI 571

Application of the hybrid complex variable method to the analysis of a crack at a piezoelectric-metal interface VOLODYMYR GOVORUKHA and MARC KAMLAH 587

1559-3959(2018)13:4;1-Y